FULL PAPER

Dalton
www.rsc.org/dalton

Lone-pair containment in closed cavities. The MTe_6O_{13} (M = Mn, Ni, Co) family of ternary oxides

John T. S. Irvine,[a] Magnus G. Johnston[b] and William T. A. Harrison*[b]

[a] *School of Chemistry, University of St Andrews, St Andrews, Fife, Scotland KY16 9ST*

[b] *Department of Chemistry, University of Aberdeen, Aberdeen, Scotland AB24 3UE. E-mail: w.harrison@abdn.ac.uk*

Received 15th January 2003, Accepted 20th May 2003
First published as an Advance Article on the web 30th May 2003

The hydrothermal and ceramic syntheses, single crystal structures and some properties of $MnTe_6O_{13}$, $NiTe_6O_{13}$ and $CoTe_6O_{13}$ are described. These isostructural phases [space group $R\bar{3}$ (No. 148) with $a \approx 10.2$ Å and $c \approx 19$ Å] contain a dense network of isolated MO_6 (M = Mn, Ni, Co) octahedra, TeO_4 folded squares and distorted TeO_{4+1} square-based pyramids, sharing vertices and edges by way of M–O–Te and Te–O–Te bonds. The Te^{IV} lone pairs are directed into closed cavities formed from 18 Te-centred and 6 MO_6 groupings. Magnetic susceptibility data for $MnTe_6O_{13}$ and $CoTe_6O_{13}$ show antiferromagnetic ordering at *ca.* 13 and 21 K, respectively, which must occur *via* a superexchange pathway.

Introduction

The crystal structures of metal tellurites are of interest because of the unpredictable coordination geometries adopted by the tellurium(IV) atoms. It has been suggested that this behavior may enhance the likelihood of a noncentrosymmetric crystal structure, with resulting useful physical properties such as second harmonic generation.[1] Crystalline tellurites also serve as models for understanding the behavior of the technologically important alkali metal–tellurite glasses.[2] Attempts to rationalize the tellurium co-ordination behavior have focused on the stereochemical activity[3] of the lone pair of electrons possessed by the Te^{IV} species, of electron configuration [Kr] $4d^{10}$ $5s^2$. Even so, the nominal tellurite grouping can crystallize in a number of ways: the simplest geometries are a TeO_3 pyramid, as seen in $Cs(VO_2)_3(TeO_3)_2$[4] or a TeO_4 folded square (or "see-saw") as seen in $BaTe_3O_7$,[5] which approximate to C_{3v} and C_{2v} local symmetry, respectively. The folded square configuration can be derived from an AX_5 trigonal bipyramid with one of the equatorial vertices missing.[6] Less regular Te/O coordinations are frequently encountered. For example, a TeO_{3+1} entity, in which one of the Te–O bonds is much longer than the other three, has been seen in the family of isostructural spiroffite $M_2Te_3O_8$ (M = Mn, Co, Ni, Cu, Zn) type phases.[7] In $Ho_2Te_5O_{13}$, one of the Te atoms shows[8] 3+2 coordination, with three short (<2 Å) and two long (2.60–2.75 Å) Te–O bonds. Occasionally,[9] the Te^{IV} lone pair shows stereochemical *inactivity*, as recently observed in the pyrochlore-type $Pr_2Te_2O_7$ which contains essentially regular $Te^{IV}O_6$ octahedra (site symmetry of Te = $\bar{3}m$).

Traditionally, mixed metal oxides containing a dense packing of atoms have been prepared in powder (microcrystalline) form by high-temperature ceramic methods.[10] However, hydrothermal or solvothermal synthesis has been used to prepare single crystals of new, condensed, metal tellurites.[7] In this paper we report the mild condition (T = 150 °C) hydrothermal syntheses, single-crystal structures and some properties of the isostructural family of phases $MnTe_6O_{13}$, $NiTe_6O_{13}$ and $CoTe_6O_{13}$. The manganese and cobalt phases were prepared as powders by ceramic syntheses some 30 years ago,[11] but no crystallographic details were established beyond unindexed powder patterns.[12]

Experimental

Hydrothermal synthesis

$MnTe_6O_{13}$ was prepared from 0.797 g (4 mmol) $MnCl_2{\cdot}4H_2O$, 1.917 g (12 mmol) TeO_2, and 15 ml H_2O. These components were sealed in a 23 ml capacity, Teflon-lined, autoclave and heated to 200 °C for eight days. After cooling the autoclave to room temperature over several hours, product recovery by vacuum filtration and washing with water resulted in a mixture of a few very light brown/pink faceted chunks of $MnTe_6O_{13}$, some clear chunks of recrystallised TeO_2 and a majority phase of white powder (identified as unreacted TeO_2 by powder diffraction). Reactions starting from a stoichiometric 1 : 6 mixture of $MnCl_2{\cdot}4H_2O$ and TeO_2 resulted in an even greater excess of unreacted/recrystallised TeO_2.

$NiTe_6O_{13}$ was prepared from 0.397 g (2 mmol) $BaCO_3$, 0.953 g (4 mmol) $NiCl_2{\cdot}6H_2O$, 0.956 g (6 mmol) TeO_2 and 15 ml H_2O. These components were sealed in an autoclave and heated to 155 °C for six days. Solid product recovery as above led to a mixture of a few sparkling yellow chunks of $NiTe_6O_{13}$ accompanied by unidentified green powder and clear blocks of TeO_2.

$CoTe_6O_{13}$ was prepared from the hydrothermal reaction (six days at 155 °C) of 0.396 g (2 mmol) $BaCO_3$, 0.952 g (4 mmol) $CoCl_2{\cdot}6H_2O$, 0.959 g (6 mmol) TeO_2 and 15 ml H_2O. Solid-product recovery as above led to a mixture of large (to 2 mm) sparkling, intense purple faceted rhombs of $CoTe_6O_{13}$ accompanied by pink powder [possibly hydrated $Co(OH)_2$] and clear blocks of TeO_2.

Ceramic synthesis

An off-white powder sample of $MnTe_6O_{13}$ was prepared from stoichiometric amounts of $MnCO_3$ and TeO_2. These components were thoroughly ground together and heated to 590 °C for six days under flowing N_2 gas with one intermediate regrinding. A clean, sharp, X-ray powder pattern in excellent accordance with a simulation of the $MnTe_6O_{13}$ single-crystal structure and the previously reported powder pattern[12] was obtained. Pale purple powder of $CoTe_6O_{13}$ was prepared from stoichiometric amounts of $CoCO_3$ and TeO_2. These components were thoroughly ground together and heated to 620 °C for 16 days in flowing N_2 with three intermediate regrindings. The resulting powder pattern corresponded to pure, highly crystalline $CoTe_6O_{13}$. We have not prepared the nickel phase by high temperature methods: variants on the ceramic syntheses described here always lead to a mixture of $NiTe_2O_5$[13] and unreacted TeO_2. Attempts to prepare $ZnTe_6O_{13}$ by ceramic methods always led to a mixture of spiroffite-type $Zn_2Te_3O_8$[7] and ZnO whilst similar syntheses aimed at $CuTe_6O_{13}$ led to a mixture of $CuTe_2O_5$ (synthetic rajite)[14] and TeO_2.

DOI: 10.1039/b300573a

Table 1 Crystallographic parameters

	$MnTe_6O_{13}$	$NiTe_6O_{13}$	$CoTe_6O_{13}$
Formula weight	1028.54	1032.31	1032.53
Crystal system	Trigonal	Trigonal	Trigonal
a/Å	10.2505 (5)	10.1522 (5)	10.1641 (5)
c/Å	19.2195 (9)	18.8669 (9)	18.9814 (9)
Z	6	6	6
Space group	$R\bar{3}$ (No. 148)	$R\bar{3}$ (No. 148)	$R\bar{3}$ (No. 148)
T/°C	25 ± 2	25 ± 2	25 ± 2
ρ_{calc}/g cm^{-3}	5.86	6.11	6.06
μ/cm^{-1}	159.2	170.9	167.4
Reflections measured	5886	5768	4461
Unique reflections	1417	1356	1364
R_{int}	0.035	0.027	0.025
Parameters	62	62	62
$R(F)$ [a]	0.022	0.022	0.023
$wR(F^2)$ [b]	0.052	0.053	0.052

[a] $R = \Sigma||F_o| - |F_c||/\Sigma\,|F_o|$ for merged reflections with $I > 2\sigma(I)$. [b] $R_w = [\Sigma\, w\,(|F_o^2| - |F_c^2|)^2/\Sigma\, w|F_o^2|^2]^{1/2}$.

Characterization

Powder X-ray data for $MnTeO_{13}$ and $CoTe_6O_{13}$ were collected on a Bruker D8 automated diffractometer (Cu Kα radiation, λ = 1.54178 Å, T = 25 °C) and analyzed using the Eva suite of programs. Room-temperature diffuse reflectance data for $MnTeO_{13}$ and $CoTe_6O_{13}$ (reference standard $BaSO_4$) were collected using a Shimadzu UV-3100 machine and converted to the Kubelka–Munk function. Variable-temperature magnetic susceptibility data for $MnTeO_{13}$ and $CoTe_6O_{13}$ were collected using a Quantum Design MPMS SQUID magnetometer in both field-cooled (FC) and zero-field-cooled (ZFC) modes. There was insufficient amount of pure $NiTe_6O_{13}$ to perform similar characterization measurements.

Structure determinations

In each case, a suitable crystal ($MnTe_6O_{13}$: very pale pink octahedron, ~0.13 × 0.12 × 0.12 mm; $NiTe_6O_{13}$: yellow rhomb ~0.17 × 0.14 × 0.13 mm; $CoTe_6O_{13}$: intense deep purple, gem-like, faceted chunk ~0.40 × 0.32 × 0.31 mm) was mounted on a thin glass fiber with cyanoacrylate adhesive, and room-temperature (20 ± 2 °C) diffraction data were collected using a Bruker SMART1000 CCD area-detector diffractometer[15] (Mo Kα radiation, λ = 0.71073 Å) as outlined in Table 1. Empirical absorption corrections were applied on the basis of multiply measured and symmetry-equivalent reflections with SADABS,[16] with resulting transmission factor ranges as follows: $MnTe_6O_{13}$ 0.394–0.566; $NiTe_6O_{13}$ 0.455–0.695; $CoTe_6O_{13}$ 0.103–0.162. The systematic absences indicated space groups $R3$, $R\bar{3}$, $R32$, $R3m$, or $R\bar{3}m$.

Direct methods[17] established enough of the $MnTe_6O_{13}$ structure to enable the remaining few oxygen atoms to be located from difference maps without difficulty as the refinement progressed. The refinements for the nickel and cobalt phases used the $MnTe_6O_{13}$ coordinates as a starting model (Mn replaced by Ni and Co, respectively). In each case, space group $R\bar{3}$ (No. 148) resulted in satisfactory refinement and was assumed thereafter. The final cycles of full-matrix least-squares refinement[18] included anisotropic temperature factors for all atoms and a secondary extinction correction. No additional crystal symmetry was evident.[19]

CCDC reference numbers 201289–201291.

See http://www.rsc.org/suppdata/dt/b3/b300573a/ for crystallographic data in CIF or other electronic format.

Results

Crystal structures

Final atomic positional and thermal parameters for the three title compounds are listed in Table 2, with selected bond distance/angle data in Tables 3 and 4.

Table 2 Atomic coordinates/thermal parameters

Atom	x	y	z	U_{eq} [a]
$MnTe_6O_{13}$				
Mn1	0.0	0.0	0.24417(4)	0.00862(16)
Te1	0.15413(3)	0.23722(3)	0.404036(11)	0.00994(7)
Te2	0.23094(2)	0.05956(3)	0.091045(11)	0.00858(7)
O1	0.0876(3)	0.2059(3)	0.30814(13)	0.0142(5)
O2	0.1968(3)	0.0486(3)	0.18604(13)	0.0131(5)
O3	0.0	0.0	0.4113(2)	0.0115(8)
O4	0.3335(3)	−0.0819(3)	0.11389(14)	0.0141(5)
O5	0.1289(3)	0.1822(3)	0.06988(14)	0.0128(5)
$NiTe_6O_{13}$				
Ni1	0.0	0.0	0.24353(4)	0.00699(15)
Te1	0.15581(3)	0.23779(3)	0.405279(12)	0.00829(8)
Te2	0.23294(2)	0.06277(3)	0.090528(12)	0.00716(8)
O1	0.0924(3)	0.2028(3)	0.30678(14)	0.0114(5)
O2	0.1937(3)	0.0542(3)	0.18726(14)	0.0104(5)
O3	0.0	0.0	0.4142(2)	0.0092(8)
O4	0.3316(3)	−0.0832(3)	0.11542(15)	0.0125(5)
O5	0.1287(3)	0.1840(3)	0.06876(15)	0.0115(5)
$CoTe_6O_{13}$				
Co1	0.0	0.0	0.24401(4)	0.00644(15)
Te1	0.15564(3)	0.23755(3)	0.404936(11)	0.00779(8)
Te2	0.23254(2)	0.06187(3)	0.090712(11)	0.00650(8)
O1	0.0895(3)	0.2034(3)	0.30747(13)	0.0111(5)
O2	0.1942(3)	0.0519(3)	0.18688(13)	0.0101(4)
O3	0.0	0.0	0.4139(2)	0.0087(7)
O4	0.3328(3)	−0.0818(3)	0.11516(14)	0.0116(5)
O5	0.1291(3)	0.1837(3)	0.06907(14)	0.0105(4)

[a] $U_{eq} = 1/3[U_1 + U_2 + U_3]$.

Table 3 Selected bond lengths (Å)

	$MnTe_6O_{13}$	$NiTe_6O_{13}$	$CoTe_6O_{13}$
M–O2 × 3	2.136(3)	2.053(2)	2.076(3)
M–O1 × 3	2.208(3)	2.148(3)	2.161(3)
Te1–O4	1.853(3)	1.857(3)	1.857(3)
Te1–O1	1.936(3)	1.940(3)	1.939(2)
Te1–O3	2.1416(4)	2.1306(4)	2.1311(4)
Te1–O1	2.179(3)	2.183(3)	2.183(3)
Te2–O2	1.852(3)	1.861(3)	1.859(2)
Te2–O5	1.922(3)	1.922(3)	1.923(3)
Te2–O5	2.039(3)	2.026(3)	2.027(3)
Te2–O4	2.219(3)	2.214(3)	2.208(3)
Te2–O2	2.615(3)	2.551(3)	2.570(3)

In $MnTe_6O_{13}$ (Figs. 1 and 2) the single crystallographically distinct Mn atom (site symmetry 3) is coordinated by three O1 and three O2 species in squashed octahedral geometry with d_{av}(Mn–O) = 2.172 (3) Å, in good accordance with the expected separation (2.19 Å) of high-spin Mn^{II} and O^{2-}, based on ionic radius sums.[20] The Te1 species has four O atom near neighbors in folded square configuration, one of which (O3) occupies a special position with 3-fold symmetry. The axial bonds to O1 and O3 are longer (d > 2.15 Å) than the equatorial bonds to O1 and O4 (d < 1.95 Å) which is typical for this type of tellurium–oxygen grouping.[7] There are four next-nearest-neighbor Te ··· O interactions at 3.007 (to O4), 3.033 Å (O2), 3.166 Å (O4), and 3.189 Å (O5); when considering all eight of these O atoms, an extremely distorted dodecahedron (Fig. 3) is formed around Te1. The Te2 species has four O atoms in close proximity (d < 2.25 Å), again approximating to folded square geometry, with a fifth, O2 atom, 2.616 Å distant. These five O atoms make up a highly distorted square-based pyramid around Te2; we term this coordination geometry TeO_{4+1}. The next-nearest oxygen atom (O5) with d(Te ··· O) = 3.128 Å completes a nominal, grossly distorted, octahedron about Te2. The idea that various Te^{IV} co-ordination geometries could be formally derived from a "TeO_6" octahedron was suggested some time ago.[21]

Table 4 Selected bond angles (°)

	$MnTe_6O_{13}$	$NiTe_6O_{13}$	$CoTe_6O_{13}$
O4–Te1–O3	83.47(10)	82.25(10)	82.68(10)
O1–Te1–O3	82.81(14)	82.99(14)	83.02(14)
O4–Te1–O1	91.90(12)	90.22(12)	90.81(11)
O1–Te1–O1	73.92(12)	74.77(12)	74.47(12)
O3–Te1–O1	154.92(12)	154.38(12)	154.76(11)
O2–Te2–O5	95.31(12)	95.26(12)	95.11(12)
O2–Te2–O5	95.42(11)	93.57(12)	94.22(11)
O5–Te2–O5	93.29(15)	93.42(16)	93.46(16)
O2–Te2–O4	84.38(11)	85.35(11)	84.90(11)
O5–Te2–O4	84.56(11)	83.01(11)	83.64(11)
O5–Te2–O4	177.81(10)	176.15(11)	176.87(11)
O2–Te2–O2	73.20(11)	74.18(11)	74.04(11)
O5–Te2–O2	166.59(10)	165.43(11)	165.88(10)
O5–Te2–O2	94.65(10)	97.17(10)	96.29(10)
O4–Te2–O2	87.39(10)	86.10(10)	86.36(10)
Te1–O1–Te1	106.08(12)	105.23(12)	105.53(12)
Te1–O1–Mn1	129.05(13)	130.80(14)	130.20(14)
Te1–O1–Mn1	122.49(12)	122.93(12)	122.61(11)
Te2–O2–Mn1	131.11(14)	132.37(15)	132.36(14)
Te2–O2–Te2	106.80(11)	105.82(11)	105.96(11)
Mn1–O2–Te2	110.38(11)	113.14(11)	111.99(10)
Te1–O3–Te1	119.58(3)	119.38(3)	119.38(3)
Te1–O4–Te2	131.56(14)	130.14(14)	130.68(14)
Te2–O5–Te2	137.13(14)	136.78(15)	136.76(14)

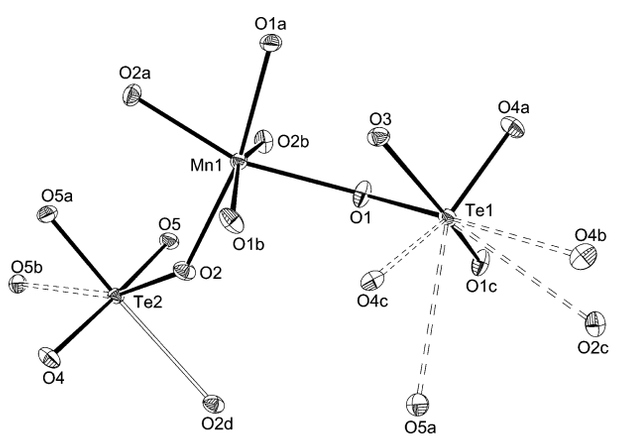

Fig. 1 View of a fragment of the $MnTe_6O_{13}$ crystal structure showing the cation coordination environments (50% thermal ellipsoids). The long Te2–O2 bond is shown as an unfilled line (see text) and the very long (d > 3Å) Te ··· O contacts are indicated by dashed lines. Symmetry generated atoms are indicated by O1a, *etc.* The structures of $NiTe_6O_{13}$ and $CoTe_6O_{13}$ are virtually identical to that of $MnTe_6O_{13}$.

The O atoms in $MnTe_6O_{13}$ adopt various co-ordinations: O1 bonds to one Mn and two Te1 in essentially planar configuration [sum of M–O–M (M = Mn, Te) bond angles = 357.6°]. O2 bonds to one Mn and two Te2 in highly squashed pyramidal geometry, and O3 bonds to three Te1 in essentially planar trigonal configuration (sum of Te–O–Te angles = 358.7°). O4 and O5 serve as simple Te–O–Te bicoordinate bridges (θ_{av} = 134.4°). Bond valence sum (BVS) calculations for the cations using the Brown formalism[22] are in fair agreement with expected values: BVS(Mn) = 2.15, BVS(Te1) = 3.74, BVS(Te2) = 4.11 (expected for Mn = 2.00, for Te = 4.00).

The polyhedral connectivity in $MnTe_6O_{13}$ results in a dense, tellurium rich, network containing isolated (from each other) MnO_6 groupings. The structure may be schematically built up as follows: the Mn and Te1-centred polyhedra combine to form infinite, honeycomb-like, sheets (Fig. 4) of hexagonal 12 rings (12 polyhedral units) arrayed normal to [001]. Each 12 ring contains six manganese nodes, and each adjacent pair of MnO_6 octahedra is fused together by a pair of Te1 moieties. Trios of Te2-centred groups cap the top and bottom of each hexagonal 12 ring resulting in an enclosed volume not containing any other chemical species (see below). The capping $Te2O_{3+1}$ groups fuse the layers into a continuous, three-dimensional structure. The rhombohedral crystal symmetry dictates that, with respect to the z direction, adjacent Mn/Te1 sheets are laterally displaced from each other by x = 1/3 and y = 2/3. Thus, the trio of Te2 groups that caps the 12 ring also bond to a single CoO_6 moiety in the next sheet and there are no continuous channels of any significant size in this structure. Finally, the structural effect of the Te^{IV} lone pairs may be considered.[23] If we assume that the Te1 lone pair occupies the "missing" equatorial vertex of a trigonal bipyramid and the Te2 lone pair occupies the missing vertex of an octahedron (see above), then both the Te1

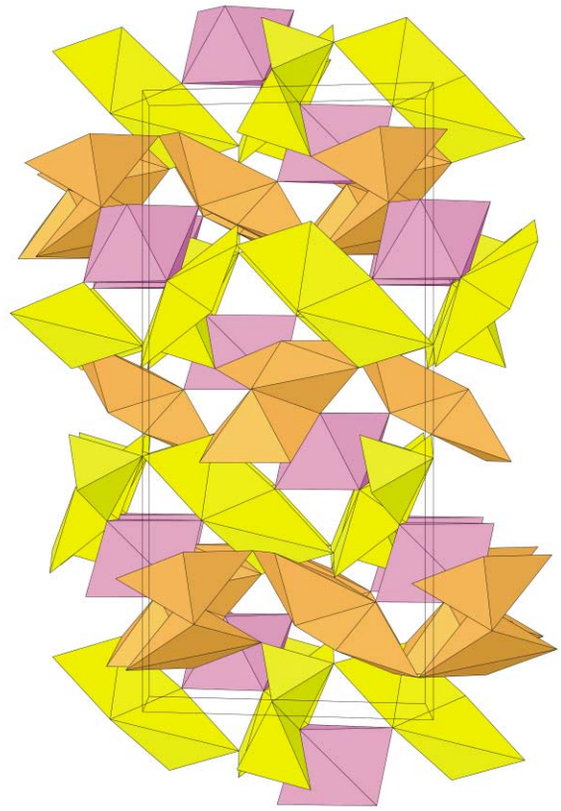

Fig. 2 Polyhedral representation of the structure of $MnTe_6O_{13}$ viewed down [100] showing the connectivity of MnO_6 octahedra (pink), $Te1O_4$ groups (yellow) and $Te2O_{4+1}$ groups (orange).

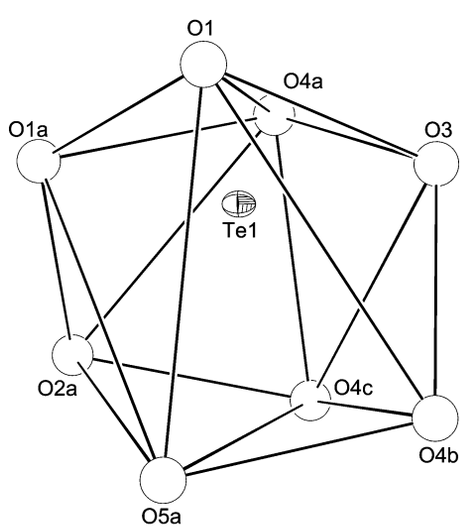

Fig. 3 Detail of the Te1 coordination environment in $MnTe_6O_{13}$ which can be regarded as a highly distorted dodecahedron. Symmetry generated atoms are indicated by O1a, *etc.*

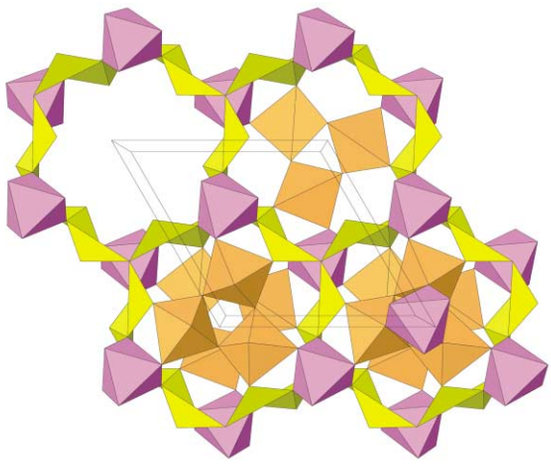

Fig. 4 View down [001] of a slab of $MnTe_6O_{13}$ showing the 12-ring honeycomb layers, built up from six MnO_6 octahedra (pink), each fused together by two $Te1O_4$ moieties (yellow). The way the $Te2O_{4+1}$ groups (orange) cap the top and bottom of each 12 ring to result in closed cavities containing the Te^{IV} lone pairs is shown sequentially: *top left*, an "empty" 12-ring hole; *top right*, a 12-ring with three $Te2O_{4+1}$ groups attached; *bottom left*, a 12 ring with $Te2O_{4+1}$ groups attached top and bottom; *bottom right*, another MnO_6 octahedron in the next Mn/Te1 layer, attached to a $Te2O_{4+1}$ trio.

and Te2 lone pairs are directed into closed, squashed cavities. The walls of the cavity are formed from a polyhedral 12 ring and the top and bottom of the cavity is formed from a trio of $Te2O_{3+1}$ groups (Fig. 4).

$NiTe_6O_{13}$ has a very similar structure to that of $MnTe_6O_{13}$. The most significant difference can be seen in the average Ni–O bond distance of 2.099 Å (expected ionic radius sum for Ni^{2+} and O^{2-} = 2.05 Å). Most of the Te–O separations are within 0.02 Å of the equivalent contacts in $MnTe_6O_{13}$ with the exception of the long Te2–O2 bond which is some 0.06 Å shorter in the nickel phase. Bond angles are within one or two degrees of their equivalent values in the manganese compound. Bond valence sums of BVS(Ni) = 1.81 (expected = 2.00), BVS(Te1) = 3.72 and BVS(Te2) = 4.14 for $NiTe_6O_{13}$ are in adequate agreement with those expected.

$CoTe_6O_{13}$ is very similar to its manganese and nickel congeners and the average Co–O bond length of 2.119 Å is more or less that expected (2.11 Å) based adding the ionic radii of high-spin Co^{II} and O^{2-}. The Te/O network is essentially identical to that of the manganese and nickel phases. Bond valence sums are as follows: BVS(Co) = 1.91 (expected = 2.00), BVS(Te1) = 3.72 and BVS(Te2) = 4.14.

Optical measurements

The diffuse reflectance spectra of $MnTe_6O_{13}$ and $CoTe_6O_{13}$ (Fig. 5) show strong absorption features at wavelengths shorter than 400nm (~3.1 eV), which, by analogy with the properties of spiroffite type phases,[7] correspond to the optical band gaps in these materials. The band gap energy (for $MnTe_6O_{13}$ 375 nm or 3.30 eV; for $CoTe_6O_{13}$ 349 nm or 3.55 eV) was estimated from the absorbance maximum half-height. The band gap of cobalt spiroffite, $Co_2Te_3O_8$, occurs at a very similar energy (3.60 eV) to that of $CoTe_6O_{13}$. The spectrum of $MnTe_6O_{13}$ is essentially featureless in the visible region, as expected for a high-spin d^5 cation, with no spin-allowed electronic transitions. Conversely, the spectrum of $CoTe_6O_{13}$ shows additional peaks in the visible region, at 754, 566, and 505 nm (shoulder) which are attributable to spin-allowed d–d transitions[24] for the d^7 Co^{2+} species.

Magnetic measurements

Magnetic susceptibility data (Fig. 6) for $MnTe_6O_{13}$ and $CoTe_6O_{13}$ indicate Curie–Weiss behaviour. A very good fit was

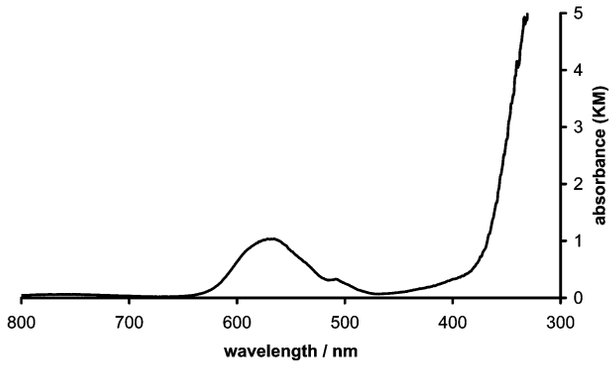

Fig. 5 Diffuse reflectance spectrum of $CoTe_6O_{13}$.

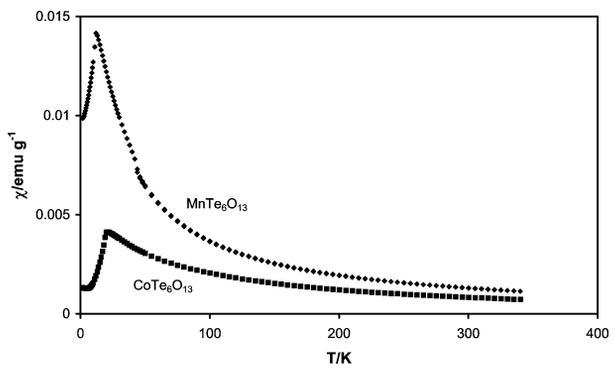

Fig. 6 Plots of magnetic susceptibility *versus* temperature for $MnTe_6O_{13}$ (diamonds) and $CoTe_6O_{13}$ (squares).

obtained with the Curie–Weiss expression for both these solids (for $MnTe_6O_{13}$ $\Theta = -11.61$ (1) K; for $CoTe_6O_{13}$, $\Theta = -38.94$ (1) K), implying low-temperature antiferromagnetic ordering of the transition metal cations in both materials, with Néel temperatures of 13 K for $MnTe_6O_{13}$ and 21 K for $CoTe_6O_{13}$. The effective magnetic moments, calculated from the paramagnetic regions of the susceptibility plots, are 5.84 and 4.80 Bohr magnetons for $MnTe_6O_{13}$ and $CoTe_6O_{13}$, respectively, which are within the expected range for high-spin d^5 (Mn^{2+}) and high-spin d^7 with appreciable spin–orbit coupling (Co^{2+}). The cation–cation interactions must occur *via* superexchange; the shortest exchange pathways in $MnTe_6O_{13}$ (6.839 Å) and $CoTe_6O_{13}$ (6.778 Å) both occur *via* a M–O1–Te1–O1–M link. The field-cooled and zero-field-cooled susceptibility traces are virtually identical for both materials, indicating the absence of any appreciable ferromagnetism or dynamic magnetic behavior.

Discussion

Mild condition hydrothermal synthesis has shown its utility as a route to single crystals of new tellurites of relatively simple stoichiometry, albeit in this case with poor yields and substantial amounts of impurities/unreacted starting materials. In the present study, one reason for this is the relative insolubility of TeO_2 in water, except at higher pH, hence the requirement for barium carbonate in the nickel and cobalt syntheses. However, high pH also causes precipitation of divalent transition metal hydroxides and/or carbonates. Thus, there is an inherent contradiction between the solubilities of the reactants as a function of pH. However, the slow dissolution rates and small solution concentrations of the component species may well assist in the formation of single crystals. Ceramic synthesis was successful in preparing pure $MnTe_6O_{13}$ and $CoTe_6O_{13}$ in accordance with previous results,[11] but $NiTe_6O_{13}$ could not be made by solid-state reaction at high temperatures, perhaps indicating that it is metastable with respect to other phases and hydrothermal synthesis is the only possible synthesis route. Interestingly, hydrothermal reactions of M^{2+}/Te/O precursors at significantly higher temperatures (375 °C) that those used here did not lead

to any MTe_6O_{13} type phases but instead produced single crystals of spiroffite ($M_2Te_3O_8$) analogues.[7]

The physical properties of the title compounds are consistent with their crystal structures and those of related compounds. The magnetic ordering temperature for $CoTe_6O_{13}$ seen here is significantly lower than that seen for $Co_2Te_3O_8$ (T_N = 70 K) which perhaps reflects the longer superexchange pathway in $CoTe_6O_{13}$.

Overall, the structures of these phases demonstrate the typical irregular coordination behavior of tellurium(IV),[1] and the strong tendency for concatenation of Te/O networks.[2] The way in which the tellurium lone pairs are accommodated in this structure type is notable: the enclosed cavities are completely different to the "self contained," one-dimensional, infinite tubes found in the tellurium-rich phases $BaTe_3O_7$ and $BaTe_4O_9$,[5] the lone-pair sheets seen in $Ni_5(TeO_3)_4X_2$ (X = Cl, Br),[25] and the one-dimensional channels seen in $Ga_2Te_4O_{11}$.[23] However, the general trend for all these phases appears to be that the Te lone pairs congregate together rather than avoid each other in space.

Acknowledgements

We thank Satish Tiwary for collecting the susceptibility data and EPSRC for provision of the SQUID magnetometer

References

1 Y. Porter, K. M. Ok, N. S. P. Bhuvanesh and P. S. Halasyamani, *Chem. Mater.*, 2001, **13**, 1910.
2 C. R. Becker, S. L. Tagg, J. C. Huffman and J. W. Zwanziger, *Inorg. Chem.*, 1997, **36**, 5559.
3 A. F. Wells, *Structural Inorganic Chemistry*, Oxford University Press, Oxford, 3rd edn., 1962, p. 890.
4 W. T. A. Harrison and J. H. N. Buttery, *Z. Anorg. Allg. Chem.*, 2000, **626**, 867.
5 M. G. Johnston and W. T. A. Harrison, *J. Am. Chem. Soc.*, 2002, **124**, 4576.
6 J. K. Burdett, *Molecular Shapes*, John Wiley, New York, 1980.
7 C. R. Feger, G. L. Schimek and J. W. Kolis, *J. Solid State Chem.*, 1999, **143**, 246.
8 F. A. Weber, S. F. Meier and T. Schleid, *Z. Anorg. Allg. Chem.*, 2001, **627**, 2225.
9 F. A. Weber and T. Schleid, *Z. Anorg. Allg. Chem.*, 2000, **626**, 1285.
10 A. R. West, *Solid State Chemistry and its Applications*, John Wiley, Chichester, 1984.
11 M. Trömel and D. Schmid, *Z. Anorg. Allg. Chem.*, 1972, **387**, 230.
12 $MnTe_6O_{13}$, JCPDS card 24–742; $CoTe_6O_{13}$, JCPDS card 24–338. In addition, $MgTe_6O_{13}$ (JCPDS card 28–634) is probably isostructural with these materials.
13 C. Platte and M. Trömel, *Acta Crystallogr., Sect. C*, 1981, **37**, 1276.
14 K. Hanke, V. Kupcik and O. Lindqvist, *Acta Crystallogr., Sect. B*, 1973, **29**, 963.
15 SMART and SAINT, Bruker Inc., Madison, WI, 1999.
16 G. M. Sheldrick, SADABS, Program for area detector adsorption correction, Institute for Inorganic Chemistry, University of Göttingen, Germany, 1996.
17 G. M. Sheldrick, SHELXS-97, Program for solution of crystal structures, University of Göttingen, Germany, 1997.
18 G. M. Sheldrick, SHELXL-97, Program for refinement of crystal structures, University of Göttingen, Germany, 1997.
19 L. G. Farugia, PLATON for Windows, University of Glasgow, Scotland, 2002.
20 R. D. Shannon, *Acta Crystallogr., Sect. A*, 1976, **32**, 751.
21 I. D. Brown, *J. Solid State Chem.*, 1974, **11**, 214.
22 I. D. Brown, *J. Appl. Crystallogr.*, 1996, **29**, 479.
23 M. Dutreilh, P. Thomas, J.-C. Champarnaud-Mesjard and B. Frit, *Solid State Sci.*, 2001, **3**, 423.
24 A. B. P. Lever, *Inorganic Electron Spectroscopy*, Elsevier, Amsterdam, 1984.
25 M. Johnsson, K. W. Törnroos, P. Lemmens and P. Millet, *Chem. Mater.*, 2003, **15**, 68.